

# RSC Advances

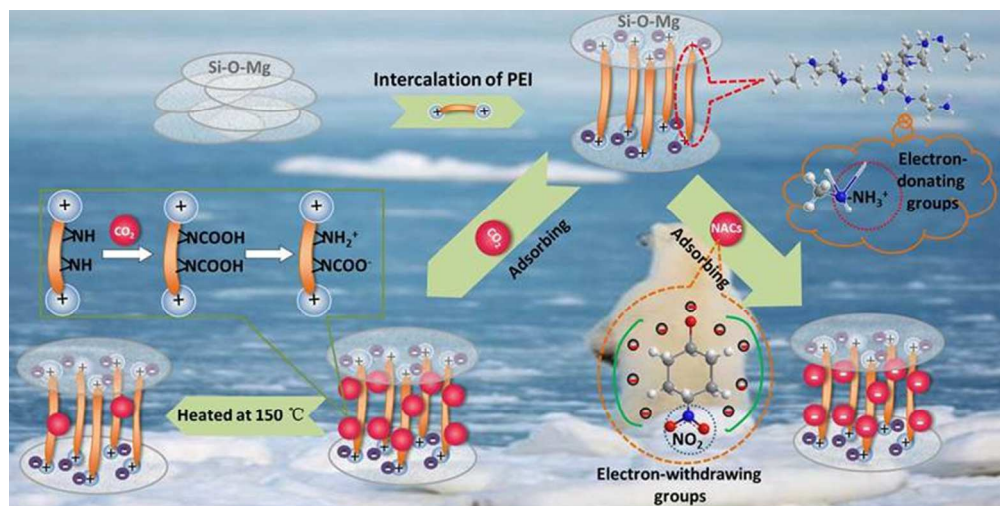


This is an *Accepted Manuscript*, which has been through the Royal Society of Chemistry peer review process and has been accepted for publication.

*Accepted Manuscripts* are published online shortly after acceptance, before technical editing, formatting and proof reading. Using this free service, authors can make their results available to the community, in citable form, before we publish the edited article. This *Accepted Manuscript* will be replaced by the edited, formatted and paginated article as soon as this is available.

You can find more information about *Accepted Manuscripts* in the [Information for Authors](#).

Please note that technical editing may introduce minor changes to the text and/or graphics, which may alter content. The journal's standard [Terms & Conditions](#) and the [Ethical guidelines](#) still apply. In no event shall the Royal Society of Chemistry be held responsible for any errors or omissions in this *Accepted Manuscript* or any consequences arising from the use of any information it contains.



136x68mm (150 x 150 DPI)

## PAPER

# PEI@Mg<sub>2</sub>SiO<sub>4</sub>: an efficient carbon dioxide and nitrophenol compounds adsorbing material

cweizhiCite this: DOI: 10.1039/x0xx00000x

Zheng-Yong Chen<sup>a</sup>, Hong-Wen Gao<sup>a</sup> and Jia-Xiang Yang<sup>a,b</sup>

The PEI@Mg<sub>2</sub>SiO<sub>4</sub> hybrid composite is readily synthesized for adsorbing carbon dioxide (CO<sub>2</sub>) and nitrophenol compounds (NACs), in which more than 11% PEI is embedded. By the removal rate of 4-nitrophenol (10 mg/L) and the capture capacity of CO<sub>2</sub>, the Mg<sup>2+</sup>: PEI: SiO<sub>3</sub><sup>2-</sup> optimal mole ratio of the PEI@Mg<sub>2</sub>SiO<sub>4</sub> is 1: 0.6: 1.5. The composite shows the highest adsorption amounts of 0.94 mmol/g CO<sub>2</sub> at 50 °C. The heat treatment regeneration exhibits a good stability, e.g. CO<sub>2</sub> capture capacity decreasing by only 20% for fourth cycles and the desorption rate of CO<sub>2</sub> remains more than 91%. It also exhibits a fast adsorption and high capacity to 4-nitrophenol (NP), 2,4-dinitrophenol (DNP) and 2,4,6-trinitrophenyl group (TNP). The adsorption capacity of NP, DNP and TNP is 2.40 mmol/g, 2.66 mmol/g and 4.85 mmol/g respectively, which are more than the conventional sorbents. This work presents a new sorbent for CO<sub>2</sub> and nitrophenol compounds with the higher capacity and eco-friendly.

Received 00th xxxx xxxx,

Accepted 00thxxxx xxxx

DOI: 10.1039/x0xx00000x

www.rsc.org/

Inorganic-organic (IO) materials with hierarchical structures and complex morphologies assembled through "host-guest" chemistry have attracted much attention for a fundamental interest in environmental science and their potential applications in water treatment and gas remediation.<sup>1</sup> It is necessary to find special properties by intercalating appointed organic material into a stable inorganic matrix. Some entity frameworks in layered architectures have been utilized as an ideal "host" supports in the construction of multifunctional adsorbents such as layered double hydroxides<sup>2</sup>, layered transition metal oxides<sup>3</sup>, graphite, and other lamellar materials<sup>4-5</sup>. In particular, layered magnesium silicate has been applied in absorbing to pollutants<sup>6</sup> because of their high surface area<sup>7-8</sup>, properties of ion exchange, hydrophobic character, adsorbant and molecular sieves<sup>9</sup>.

As a guest, surfactants and block-copolymers often are used extensively in the shape-controlled synthesis of various functional materials, where it plays a soft template or stabilizer role<sup>10-11</sup>. Among the potential "guest" molecules, diverse amine species have prospective absorption of applications in heavy metal<sup>12</sup>, organic contamination<sup>13</sup>, gaseous pollutants<sup>14</sup> and other fields. Polyethyleneimine (PEI) can effectively adsorb pollutants due to the high amine density, accessible primary amine sites on chain ends and good water-solubility<sup>15</sup>. However, before being used in the absorption for pollutants, the water-soluble PEI must be processed into a solid form. Fortunately, the combination of PEI with inorganic matrix may achieve this goal<sup>16</sup>. For example, Deng<sup>17</sup> and Ting reported that the fungal biomass with PEI-grafting showed high sorption capacity for anionic Cr(VI) and Cr(III); Tailor<sup>18</sup> and co-workers found that the MCM-41-supported modified PEI markedly increased the SO<sub>2</sub> capture capacity than that of traditional adsorbents; Gao *et al*<sup>19</sup> introduced an interesting study for adsorbing phenol perfectly with modified diatomite by PEI impregnating.

Owing to the burning of fossil fuels and various chemical processes, there is huge amounts of emission of CO<sub>2</sub> into the atmosphere, which is greenhouse gases<sup>20</sup>. More and more people believe that the anthropogenic emissions of greenhouse gases allow radiative forcing and contribute to global warming and climate change<sup>21-22</sup>. Meanwhile, the widespread of NACs in water is a main concern that impels researchers to look for remedies<sup>23-26</sup>. These compounds, in particular, nitrobenzene, their transformation products in the environment occur as contaminants worldwide and are known to be hazardous to ecological and human health<sup>27-29</sup>. Amine-layered IO materials has been shown to be successful for the removal of CO<sub>2</sub> and NACs, such as amine-layered LDHs<sup>30</sup>, amine-functionalized mesoporous silica<sup>31</sup> and milli-sized calcium<sup>32</sup>. Currently, there are two main classes of such the amine-based IO materials: (a) amines covalently bound to the support *via* the use of chemical grafting<sup>33-35</sup> and (b) physically impregnated into the support based on a "wet impregnation" method<sup>31, 36-39</sup>. The sorbents mentioned above have some obvious disadvantages, involving lacking of stability, relatively low efficiency, less content of functional compound, and poor regeneration stability<sup>40</sup>. Our previous studies indicate that the layered IO material by coprecipitation technique has a great effect on overcoming those disadvantages<sup>7, 35, 43-45</sup>. Therefore, there is a significant and untapped opportunity to improve the adsorption characteristics by developing the PEI-layered magnesium silicate material by coprecipitation technique. The objective of this study is (1) to form a hybrid material (PEI@Mg<sub>2</sub>SiO<sub>4</sub>) by coprecipitation technique (2) to utilize the high amine density and positive charge of the PEI@Mg<sub>2</sub>SiO<sub>4</sub> to adsorb NACs and CO<sub>2</sub> and (3) to investigate their resultant adsorptions. The results indicate that the PEI@Mg<sub>2</sub>SiO<sub>4</sub> is promising to capture CO<sub>2</sub> and adsorb NACs from wastewater decently.

## Experimental section

### Apparatus and Materials

The infrared spectra were measured with a Fourier transform infrared spectrometer (Model NICOLET 5700, Thermo Electron Co., USA) to indicate PEI embedded into the hybrid materials and NAC adsorbed into the sorbent. The heat weight change of the materials was performed with a thermal gravimetric analyser (Model NETZSCH TG 209 F1, NETZSCH-Geratebau GmbH, Germany). A scanning electronic microscopy (SEM) (Model Quanta 200 FEG, FEI Co., USA) was used to measure the size and shape of the hybrid sorbents. A transmission electron microscopy (TEM) (Model TECNAI G2, S-TWIN, FEI Co., USA) was used to characterize the morphology of the PEI@Mg<sub>2</sub>SiO<sub>4</sub> and Mg<sub>2</sub>SiO<sub>4</sub>. A ζ-potential instrument (Zetasizer Nano Z, Malvern, UK) was used to determine the surface potential of the sorbents. The surface area of the materials was measured with a surface area and porosimetry analyser (Model ASAP2020, Micromeritics Co., USA). The small-angle X-ray diffraction (SAXRD) (Model D/Max-2550 PC, Japan) was recorded using CuK radiation at a voltage of 30 kV and current of 50 mA and the wide-angle X-ray diffraction (WAXRD) (Model Bruker D8 Advance, Germany) in range of ~10 – 90° 2θ at 40 kV and 40 mA. The elemental analysis device (Model Vario EL III, Germany) used to determine C, N and H content of hybrid composite. A photodiode array spectrometer (Model S4100, Scinco, Korea) with the Labpro plus software (Firmware Version 060105) was used to determine the concentration of various NAC solutions.

Sodium metasilicate and magnesium nitrate (Aladdin Agents, China), sodium hydroxide (Aladdin Agents, China), PEI (M.W. 600, Aladdin Agents, China), sodium chloride (Aladdin Agents, China), hydrochloric acid (Sinopharm Chemical Reagent Co., Ltd, China) were used. The adsorptions of five phenolic compounds (Aladdin Agents, China) on the PEI@Mg<sub>2</sub>SiO<sub>4</sub> were investigated, which was NP, DNP, TNP, *p*-cresol and *p*-chlorophenol respectively.

### Synthesis of the PEI@Mg<sub>2</sub>SiO<sub>4</sub> Hybrid Composite and Mg<sub>2</sub>SiO<sub>4</sub>

2.0 g of magnesium chloride hexahydrate (AR, Aladdin Reagents Co., China) was dispersed into 100 mL of deionized water and mixed with 2.0 g ethylene imine polymer (M.W. 600, 99%, Aladdin Reagents Co., China) for 10 min with an ultrasonic fragmentation device (Model JY92-II, Xinzhi Biotechnol. Co, Ltd, Ningbo, China). 100 mL of 4.3% (w/v) sodium silicate was added rapidly under stirring. After stationarily aging for 24 h, the hybrid composite was washed repeatedly with deionized water to remove the excessive PEI. The PEI@Mg<sub>2</sub>SiO<sub>4</sub> suspension liquid was used to dry by freezer dryer. As reference, magnesium silicate was prepared according to the same procedure. The PEI@Mg<sub>2</sub>SiO<sub>4</sub> and Mg<sub>2</sub>SiO<sub>4</sub> powder were used to adsorb CO<sub>2</sub> respectively. The PEI@Mg<sub>2</sub>SiO<sub>4</sub> suspension liquid was used to adsorb NACs.

### Adsorption of CO<sub>2</sub> to the PEI@Mg<sub>2</sub>SiO<sub>4</sub> and Mg<sub>2</sub>SiO<sub>4</sub> Material

The amount of adopted CO<sub>2</sub> was determined by using a thermal gravimetric analyzer (Model NETZSCH TG 209 F1, NETZSCH-Geratebau GmbH, Germany). In a typical measurement procedure, the sample was degassed at 150 °C for 30 min in N<sub>2</sub> to remove any physically adsorbed molecules, after the temperature was decreased to 25 °C, the sample was allowed to adsorb CO<sub>2</sub> by passing CO<sub>2</sub> at a flow rate of 30 mL/min.

The influences of time and temperature on the adsorption of CO<sub>2</sub> were tested by using a thermal gravimetric analyzer (Model NETZSCH TG 209 F1, NETZSCH-Geratebau GmbH, Germany). In a typical measurement procedure, the sample was degassed at 150 °C for 30 min in N<sub>2</sub> to remove any physically adsorbed molecules, after the temperature was decreased to 50 °C, the sample was allowed to adsorb CO<sub>2</sub> by passing CO<sub>2</sub> at a flow rate of 30 mL/min, the process was continued for 40 min. The temperature of sample was adjusted from 25 °C to 100 °C. The adsorption/desorption cycling was also measured. The sample after adsorption of CO<sub>2</sub> was heated at 150 °C with a ramp rate of 5 °C/min in a nitrogen atmosphere, and then the sample was kept at this temperature for 100 min to remove the adsorbed CO<sub>2</sub>. After the temperature was decreased to 50 °C, the sample was allowed to adsorb CO<sub>2</sub> again by re-passing CO<sub>2</sub> at a flow rate of 30 mL/min, the process was continued for another 80 min, the process was repeated for four times.

### Adsorption of NACs and Phenols

The adsorption capacities of the PEI@Mg<sub>2</sub>SiO<sub>4</sub> to three kinds of NACs and two kinds of phenols were determined. The 0.02% (w: v) of the PEI@Mg<sub>2</sub>SiO<sub>4</sub> was added into the NACs and solutions of phenols e.g. DNP from 15 to 100 mg/L, TNP from 20 to 150 mg/L, *p*-cresol from 20 to 300 mg/L, NP from 50 to 420 mg/L and *p*-chlorophenol from 60 to 600 mg/L. The procedure was followed. The PEI@Mg<sub>2</sub>SiO<sub>4</sub>-pollutants liquids were mixed for 10 min by ultrasound. After the mixtures were centrifuged, the concentrations of pollutants in the supernatants were determined by spectrophotometry.

In addition, the influences of pH, ionic strength and time on the adsorption of NP (53 mg/L), DNP (19 mg/L) and TNP (20 mg/L) on the PEI@Mg<sub>2</sub>SiO<sub>4</sub> were investigated respectively. NaCl (1 M) was used to adjust ionic strength of the liquids from 0 to 0.2 M. The sorption time was carried out from 0 to 30 min. The pH was carried out from 4 to 10. In all the experiments, the pollutants in the supernatants were determined by spectrophotometry.

## Results and discussion

### Interaction of PEI with Magnesium Silicate

Our previous study indicates that the initial optimal mole ratio of Mg<sup>2+</sup>: SiO<sub>3</sub><sup>2-</sup> is 1 : 1.5 for preparing the organics-layered magnesium silicate.<sup>6</sup> From the interaction of PEI with *in-situ* formed magnesium silicate, embedded amount of PEI increases with increase of SiO<sub>3</sub><sup>2-</sup> and then the embedded amount of PEI approaches equilibrium.<sup>6</sup> The hybridization obeys the Langmuir isotherm model (Fig. 1A, 1B), e.g.  $1/q_e = 1/(K_a c_e q_\infty) + 1/q_\infty$ , where  $c_e$  is the equilibrium molarity of PEI in g/L,  $q_e$  the amount of PEI binding to magnesium silicate in mg/g,  $q_\infty$  the saturation amount of PEI in mg/g and  $K_a$  the binding constant. The  $q_\infty$  of PEI is calculated 0.41 g per gram of magnesium silicate, i.e. the

content maximum of embedded PEI in the PEI@Mg<sub>2</sub>SiO<sub>4</sub> approaches 29.4%, which is more than other results of previous similar studies.<sup>19, 45-46</sup> During the growing of Mg–O–Si particles, the positively charged amino group of PEI can bind to the negatively charged Mg–O–Si ones *via* the electrical attraction.

The ζ-potential of the magnesium silicate-only is determined to be -45.5 mV in aqueous media, which may be attributed to the fact that lots of OH<sup>-</sup> in basic media are adsorbed *via* the interaction with Mg<sup>2+</sup> and O–Si.<sup>47</sup>

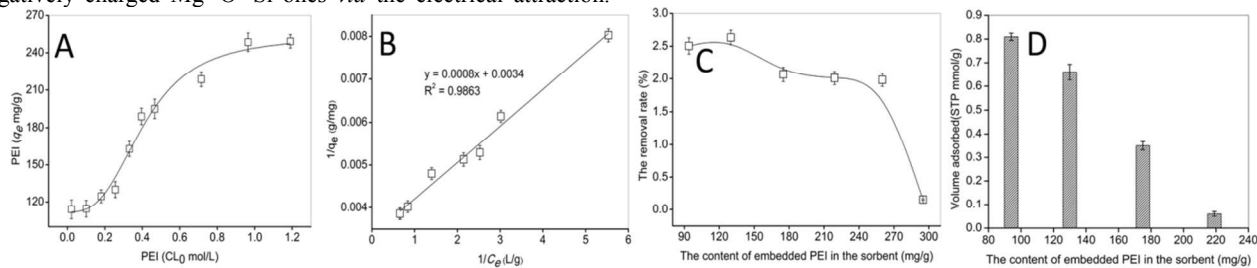


**Fig. 1** Effect of PEI on the hybridization. A: plots  $q_e$  vs  $c_0$ , B: Plots  $c_0/q_e$  vs  $c_0$ . C: the removal rate of NP with the different content of embedded PEI in the sorbent. D: the adsorption of CO<sub>2</sub> with the different content of embedded PEI in the sorbent.

However, the results of previous studies show that there is a substantial decrease in the adsorption capacity of IO-sorbent with the increasing of the content of embedded PEI, due to partial blockage of pores by the grafted amine molecules.<sup>46, 48-49</sup> In order to optimize the ratio of PEI in the PEI@Mg<sub>2</sub>SiO<sub>4</sub>, CO<sub>2</sub> and NP (10 mg/L) is selected as a representative to measure the optimal pollutant adsorption capacity of the different content of embedded PEI in the PEI@Mg<sub>2</sub>SiO<sub>4</sub>, e.g. 94 mg/g, 130 mg/g, 175 mg/g, 219 mg/g, 260 mg/g and 295 mg/g, respectively. As a result, the removal rates of NP are 2.50 %, 2.63 %, 2.07 %, 2.01 %, 1.98 % and 0.16%, which is got by using the above corresponding PEI@Mg<sub>2</sub>SiO<sub>4</sub> (Fig. 1C). The adsorptions of CO<sub>2</sub> are 0.81 mmol/g, 0.66 mmol/g, 0.35 mmol/g, 0.06 mmol, 0 mmol and 0 mmol/g respectively (Fig. 1D). Thus the adsorption of NP and CO<sub>2</sub> are maximal on the adsorbents with the Mg<sup>2+</sup>: PEI: SiO<sub>3</sub><sup>2-</sup> ratio of 1: 0.6: 1.5. The PEI@Mg<sub>2</sub>SiO<sub>4</sub> is formed and used. The molar ratio of Mg to PEI and Si in the PEI@Mg<sub>2</sub>SiO<sub>4</sub> is calculated 1: 0.13: 1.3 determined with element analysis and ICP.

### Characterization of the PEI@Mg<sub>2</sub>SiO<sub>4</sub>

An initial estimate of PEI bilayer content in the PEI@Mg<sub>2</sub>SiO<sub>4</sub> is obtained from infrared spectra (IR). As shown in Fig. 2A, the Si–O absorption peak is at 1059 cm<sup>-1</sup>. The absorption peaks at 2935 (C–H stretching), 2819 (C–H stretching), 1756 (–NH<sub>2</sub> and –NH– deformation), 1472 (–NH<sub>2</sub> and –NH– deformation) and 1290 (–NH<sub>2</sub> and –NH– deformation) cm<sup>-1</sup> indicate that PEI is embedded into the PEI@Mg<sub>2</sub>SiO<sub>4</sub>. From the element analysis of the PEI@Mg<sub>2</sub>SiO<sub>4</sub>, both 7.1% C and 3.8% N indicate that 11.4% PEI is embedded into the PEI@Mg<sub>2</sub>SiO<sub>4</sub> (Table S1, ESI†). From the small-angle XRD (SAXRD) (curve 2 in Fig. 2B), the PEI@Mg<sub>2</sub>SiO<sub>4</sub> composite possesses the layered structure. During the synthesis, the positively charged amino group of PEI (structured in Fig. 2B) can bind to the negatively charged Mg–O–Si particles *via* the electrical attraction. The ζ-potential of Mg<sub>2</sub>SiO<sub>4</sub>-only is determined to be -45.5 mV in aqueous media,

which may be attributed to the fact that lots of OH<sup>-</sup> in basic media are adsorbed *via* the interaction with Mg<sup>2+</sup> and O–Si<sup>47</sup>. After the intercalation of PEI, the ζ-potential of the PEI@Mg<sub>2</sub>SiO<sub>4</sub> changes to +15.9 mV. The electrostatic interaction occurs between PEI<sup>+</sup> and magnesium silicate. In addition, the alkyl chain (–[CH<sub>2</sub>–CH<sub>2</sub>–NH]<sub>n</sub>) of PEI in length of 3.4 nm may be embedded into two Mg<sub>2</sub>SiO<sub>4</sub>-sheets. PEI is fixed between Mg<sub>2</sub>SiO<sub>4</sub> particles in the interval of 3.9 nm (Fig. 2B).

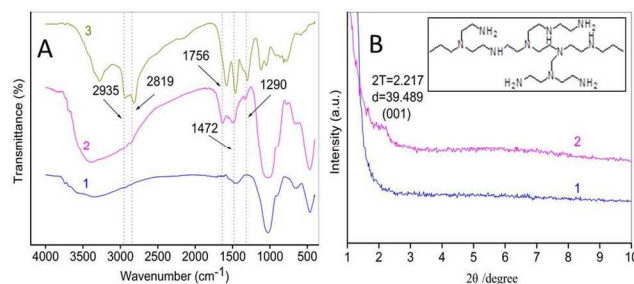


**Fig. 2** IR spectra (A) of Mg<sub>2</sub>SiO<sub>4</sub> (1), the PEI@Mg<sub>2</sub>SiO<sub>4</sub> (2) and PEI (3) and SAXRD (B) of Mg<sub>2</sub>SiO<sub>4</sub> (1) and the PEI@Mg<sub>2</sub>SiO<sub>4</sub> (2).

As shown in Fig. 3, the PEI@Mg<sub>2</sub>SiO<sub>4</sub> shows the sheet morphology with an average diameter of 40 to 60 nm (Fig. 3B), which is similar to that of Mg<sub>2</sub>SiO<sub>4</sub> (Fig. 3D). However, the PEI@Mg<sub>2</sub>SiO<sub>4</sub> also shows the layer structure (Fig. 3A) because two sheets of Mg<sub>2</sub>SiO<sub>4</sub> are aged into the layer-by-layer material by electric attraction. Meanwhile, the width of silt is about 4 nm (Fig. 3A,C), which is consistent with the SAXRD. As shown in the SEM images (Fig. 3E,F), the PEI@Mg<sub>2</sub>SiO<sub>4</sub> has flaky structure with an average diameter of 60 to 100 nm while Mg<sub>2</sub>SiO<sub>4</sub> has the granule structure with the average diameter of 60 to 80 nm (Fig. 3G). The presence of PEI affects the stacking of lamellar Mg<sub>2</sub>SiO<sub>4</sub>, which is just stringed by the intermolecular action with PEI<sup>6</sup>. The PEI in interior of the hybrid is also confirmed by the EDX (Fig. S1, ESI†).

## PAPER

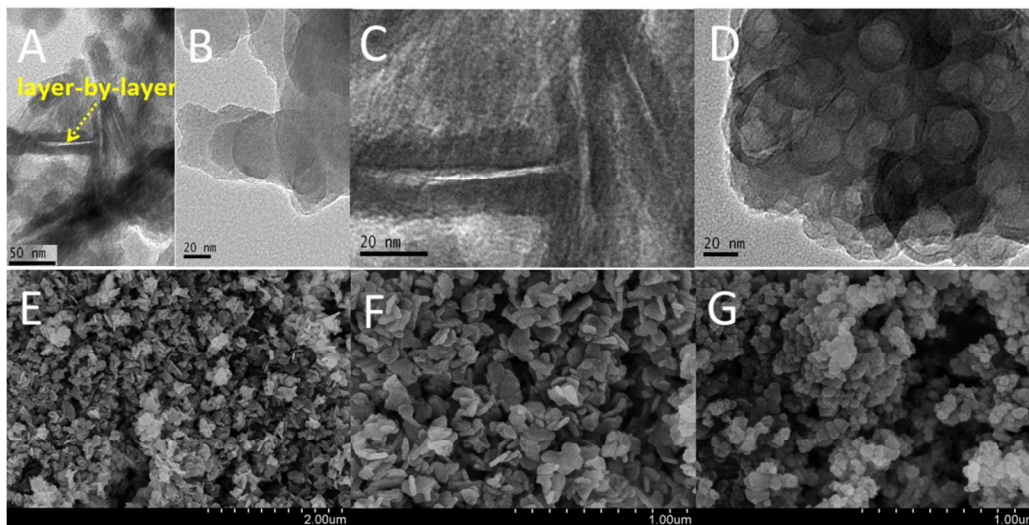


Fig. 3 TEM images of the PEI@Mg<sub>2</sub>SiO<sub>4</sub> (A, B, C) and Mg<sub>2</sub>SiO<sub>4</sub> (D). SEM of the PEI@Mg<sub>2</sub>SiO<sub>4</sub> (E, F) and Mg<sub>2</sub>SiO<sub>4</sub> (G).

Fig. 4 illustrates the N<sub>2</sub> sorption isotherm and the pore-size distribution with Barrett–Joyner–Halenda method of Mg<sub>2</sub>SiO<sub>4</sub> and the PEI@Mg<sub>2</sub>SiO<sub>4</sub>. All of the isotherms are classical type IV, which refers to the mesoporous materials. Furthermore, the isotherms have two hysteresis loops, indicating a bimodal pore size distribution in the mesoporous regions. The shapes of the two hysteresis loops are different from each other<sup>50</sup>. At the high relative pressure between 0.8 and 0.9, the hysteresis loops are type H1, suggesting the presence of cylindrical mesopores<sup>51</sup>. The above bimodal pore-size distribution is further confirmed by the pore-size distribution in Fig. 4a,b. From the pore plots, no peak appeared in the pore, indicating the presence of irregular mesopores. The mesopores may be formed by the stacking of lamellar Mg<sub>2</sub>SiO<sub>4</sub>. The BET analysis of the materials indicate that the specific surface area of Mg<sub>2</sub>SiO<sub>4</sub> and PEI@Mg<sub>2</sub>SiO<sub>4</sub> is determined to be 51.61 and 89.51 m<sup>2</sup>/g. The increased area should be contributed to the partial impregnation of PEI into Mg<sub>2</sub>SiO<sub>4</sub>.

As seen in the thermal gravimetric analysis (TGA) differential thermal gravity of the PEI@Mg<sub>2</sub>SiO<sub>4</sub> (Fig. S2, ESI†), the first step in the range of 40 to 200 °C is attributed to the removal of the physisorbed water and interlayer water, the second step in the range of 200 to 400 °C due to the removal of layer silicate and the third step in the range of 400 to 600 °C due to the removal of interlayer PEI. At 700 °C, the weight loss of the PEI@Mg<sub>2</sub>SiO<sub>4</sub> is 33.2%, where the physisorbed water, layer silicate and interlayer PEI distributed 15.0, 7.9 and 10.3% respectively, approaching that obtained from the element analysis.

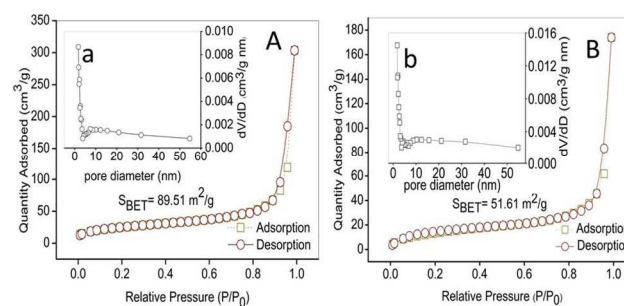
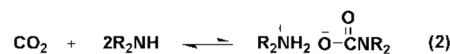
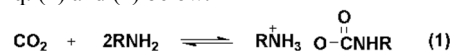


Fig. 4 N<sub>2</sub> absorption–desorption isotherm and pore-size distribution (inset) for Mg<sub>2</sub>SiO<sub>4</sub> (A, a) and the PEI@Mg<sub>2</sub>SiO<sub>4</sub> (B, b).

#### Prediction of CO<sub>2</sub> Adsorption Uptakes in the PEI@Mg<sub>2</sub>SiO<sub>4</sub>

The CO<sub>2</sub> capture capacity of Mg<sub>2</sub>SiO<sub>4</sub> and the PEI@Mg<sub>2</sub>SiO<sub>4</sub> materials is measured at 25 °C by using a thermal gravimetric analyzer. The chemisorption of CO<sub>2</sub> may occur through the formation of carbamate by the reaction of the secondary amine group (R<sub>2</sub>NH) and primary amine (RNH<sub>2</sub>) of PEI with CO<sub>2</sub>, as shown in Eq. (1) and (2) below.



It suggests that CO<sub>2</sub> would form a weak chemical bond with the secondary amine group, and subsequently lead to the formation of carbamate zwitterions<sup>52</sup>. The CO<sub>2</sub> capture capacity on Mg<sub>2</sub>SiO<sub>4</sub> is around 0.69 mmol/g, which is higher than that of the results reported<sup>30, 53–54</sup>. The interlayer anions in Mg<sub>2</sub>SiO<sub>4</sub> is favourable to CO<sub>2</sub> capture<sup>31, 55</sup>. The CO<sub>2</sub> capture capacity increases up to 0.75 mmol/g with the PEI@Mg<sub>2</sub>SiO<sub>4</sub>. This competing kinetic (diffusion) and thermodynamic (adsorption) effects has been observed and reported previously<sup>45, 53</sup>. The nanopores of the PEI@Mg<sub>2</sub>SiO<sub>4</sub> provide CO<sub>2</sub> with a diffusion path, where PEI

located on the nanopore wall offers the active adsorption sites.

For CO<sub>2</sub> capture, any adsorbent should have not only a high sorption capacity but also a fast adsorption to be energy-efficient<sup>56</sup>. A recent study demonstrated the high loading of amine may hamper the adsorption kinetics but increase the capacity<sup>57</sup>. A double-exponential model (DEM) is applied to describe the CO<sub>2</sub> adsorption kinetics on the PEI@Mg<sub>2</sub>SiO<sub>4</sub>, expressed by the relation:

$$q_t = q_e - D_1 \exp(-K_1 t) - D_2 \exp(-K_2 t) \quad (3)$$

where  $D_1$  (mg/g) and  $K_1$  (min<sup>-1</sup>) are the adsorption rate and diffusion parameter for the fast step, and  $D_2$  and  $K_2$  those for the slow step. The model is suitable for adsorbent with two different types of adsorption sites, and the adsorption contains fast and slow adsorption steps<sup>56, 58</sup>. The experimental data are fitted by the DEM model at 25, 50, 75 and 100 °C (Fig. 5A). Both  $D_1$  and  $D_2$  first increase and then decrease with increase of temperature from 25 to 100 °C and the highest value appeared at 50 °C (Table S1, ESI<sup>†</sup>). At 100 and 75 °C, the CO<sub>2</sub> adsorption equilibrium reached within 5 min. With decrease of temperature, the adsorption of CO<sub>2</sub> goes slow on the PEI@Mg<sub>2</sub>SiO<sub>4</sub>. The slow adsorption is much more obvious at 25 and 50 °C and the equilibrium have not reached at 15 min. This demonstrates a strong diffusion of CO<sub>2</sub> is hindered by PEI phase at low temperature<sup>57</sup>, proved from the diffusion parameter ( $K_1$ ,  $K_2$ ) (Table S2, ESI<sup>†</sup>). Evidently, the PEI@Mg<sub>2</sub>SiO<sub>4</sub> exhibits the highest adsorption for CO<sub>2</sub> at 50 °C. The kinetic results are also consistent with previous reports<sup>56</sup>. It may provide a valuable application to collect CO<sub>2</sub> from flue gas. In addition, the CO<sub>2</sub> adsorption equilibrium on the PEI@Mg<sub>2</sub>SiO<sub>4</sub> is completed in 18 min while that on Mg<sub>2</sub>SiO<sub>4</sub> in 35 min (Fig. S3, ESI<sup>†</sup>). The adsorption time is close to other types of adsorbent<sup>10, 56, 59-60</sup>.

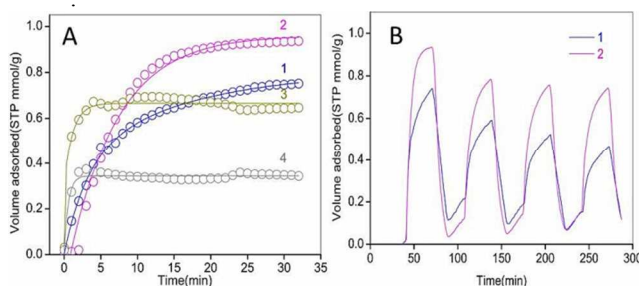


**Fig. 5** A: The CO<sub>2</sub> adsorption kinetics of the PEI@Mg<sub>2</sub>SiO<sub>4</sub> at 25 °C (1), 50 °C (2), 75 °C (3) and 100 °C (4) fitting by DEM. B: Cycles of CO<sub>2</sub> adsorption/desorption for Mg<sub>2</sub>SiO<sub>4</sub> (1) and the PEI@Mg<sub>2</sub>SiO<sub>4</sub> at 50 °C.

The successive CO<sub>2</sub> adsorption-desorption cycle may provide an assessment of the regeneration stability of the materials. The trend of cycle curves is consistent with that of other studies<sup>53, 61-62</sup> (Fig. 5B). During four cycles, the CO<sub>2</sub> capture amounts decrease from 0.94 to 0.75 mmol/g with the PEI@Mg<sub>2</sub>SiO<sub>4</sub> but from 0.74 to only 0.46 mmol/g with Mg<sub>2</sub>SiO<sub>4</sub>. The CO<sub>2</sub> adsorption capacity of the PEI@Mg<sub>2</sub>SiO<sub>4</sub> regenerated decreases by only 15 to 20%. In addition, from curve 1 more than 18% CO<sub>2</sub> is always left on the Mg<sub>2</sub>SiO<sub>4</sub> every cycle. On the contrary, from curve 2 the desorption rate of CO<sub>2</sub> remains more than 91% with the

PEI@Mg<sub>2</sub>SiO<sub>4</sub>.

### Prediction of NACs Adsorption Uptakes in the PEI@Mg<sub>2</sub>SiO<sub>4</sub>

As described the above, the PEI@Mg<sub>2</sub>SiO<sub>4</sub> carries a great deal of positive charges. It may adsorb strongly NACs, e.g. NP, DNP and TNP *via* the electric attraction. Moreover, there are many the electron-withdrawing groups (nitro group) in NACs, which is in favour of being adsorbed by the PEI@Mg<sub>2</sub>SiO<sub>4</sub>. The NP, DNP and TNP are tried to be adsorbed by the PEI@Mg<sub>2</sub>SiO<sub>4</sub> hybrid composite and the adsorption obeys the Langmuir isotherm model (Fig. 6B),  $1/q_e = 1/(K_a C_0 q_\infty) + 1/q_\infty$ . From Table 1,  $q_\infty$  value is positively related to  $\lg K_{o/w}$  value e.g. 2.40 mmol/g for NP ( $\lg K_{o/w} = 1.91$ ), 2.66 mmol/g for DNP ( $\lg K_{o/w} = 1.54$ ), 4.85 mmol/g for TNP ( $\lg K_{o/w} = 2.03$ ), which is superior to the other traditional absorbents.<sup>63-67</sup> The  $\zeta$ -potential of the hybrid composite approaches +7.29 mV, +6.43 mV and -0.39 mV after adsorption of NP, DNP and TNP respectively. The +/- charge attraction plays a primary role in the adsorption of NACs,<sup>6</sup> i.e. PEI embedding into the hybrid composite captured NACs from aqueous solution.

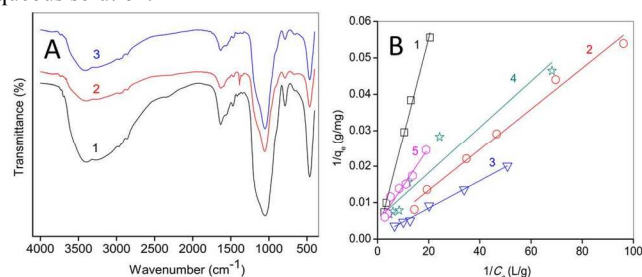


**Fig. 6** IR spectra (A) of the PEI@Mg<sub>2</sub>SiO<sub>4</sub>-NP (1), the PEI@Mg<sub>2</sub>SiO<sub>4</sub>-DNP (2), the PEI@Mg<sub>2</sub>SiO<sub>4</sub>-TNP (3), the PEI@Mg<sub>2</sub>SiO<sub>4</sub> (4), Mg<sub>2</sub>SiO<sub>4</sub> (5) and adsorption of NP (B1), DNP (B2), TNP (B3), *p*-cresol (B4) and *p*-chlorophenol (B5).

Nitro groups can increase the electronegativity of the phenolic hydroxy groups so that the amino groups of PEI@Mg<sub>2</sub>SiO<sub>4</sub> can combine with the phenolic hydroxy groups of NACs more efficiently.<sup>68</sup> Such NACs with more nitro groups often exhibit the higher adsorption capacity. In addition, the electron-withdrawing effect of chlorine group is less than nitro groups. Methyl groups can reduce the electronegativity of the phenolic hydroxy groups, which weights against the combination between the amino groups of the PEI@Mg<sub>2</sub>SiO<sub>4</sub> and the phenolic hydroxy groups of *p*-cresol. Therefore, the absorption ability of pollutants from high to low is: TNP > DNP > NP > *p*-chlorophenol > *p*-cresol. The  $\lg(K_a)$  values of NP, DNP and TNP are calculated to be 2.52, 2.66 and 3.05 respectively, which are superior to their  $\lg K_{o/w}$ . And there are many long hydrophobic chains i.e.  $-\text{[CH}_2\text{-CH}_2\text{-N}^+\text{]}_n$  in PEI, which indicates the PEI@Mg<sub>2</sub>SiO<sub>4</sub> carries decent hydrophobicity<sup>69</sup>. Therefore, the hydrophobic interaction occurs between the hydrophobic groups of NACs and the long alkyl chains of embedded PEI in the PEI@Mg<sub>2</sub>SiO<sub>4</sub> besides the electrical charge interaction.

## PAPER

**Table 1** The adsorption capacity of the PEI@Mg<sub>2</sub>SiO<sub>4</sub> to NACs with  $K_a$  and comparison with the other sorbents reported

Pollutants	Group category	Nitro groups number, $n$	$q_\infty$		$\lg K_a$	$R^2$	$q_\infty$ comparison	
			mmol/g	mg/g			Sorbent	$q_\infty$ / mg/g
TNP	electron-withdrawing groups	3	4.85	1111	3.05	0.9962	hydrotalcite	504 <sup>63</sup>
DNP		2	2.66	455	2.66	0.9884	activated carbon fibers	417 <sup>64</sup>
NP		1	2.40	333	2.52	0.9763	granular activated carbon	206 <sup>65</sup>
<i>p</i> -chlorophenol		/	2.23	286	2.47	0.9767	/	/
<i>p</i> -cresol	electron-donating groups	/	1.68	182	2.26	0.9398	/	/

On the basis of the above experiments, we further carried out *in situ* IR experiments to clarify the NACs kinetics on the adsorbents. *In situ* IR difference spectra upon NACs adsorption, the absorption peaks of nitro groups at 1385 to 1565 cm<sup>-1</sup> indicate that NACs are embedded into the hybrid materials (Fig. 6A). The pH of solution affected obviously the adsorption of NACs. With increasing pH 4 to 6, the  $q_e$  of NP and DNP increase by 50% and 215% respectively and remains almost constant between pH 7 to 10. The  $q_e$  of TNP increases by 20% between pH 4 to 6 and decreases by 37% at pH 10 (Fig. S4, ESI<sup>†</sup>). The adsorption of NACs increased slightly with increase of ionic strength. It is attributed to the fact that the protonation of PEI is triggered in strong acid.<sup>70</sup> The  $q_e$  of NP, DNP and TNP increases by 16%, 4% and 13% respectively in 0.25 M NaCl (Fig. S5, ESI<sup>†</sup>). It is attributed to the fact that ionic strength can strengthen the hydrophobic interaction between NACs and PEI. The adsorption equilibrium is completed in 8 min (Fig. S6, ESI<sup>†</sup>), which is much faster than that of activated carbon<sup>71</sup>. Therefore, the hybrid sorbent prepared is favorable for treatment of the highly salt and slightly alkaline wastewater.

## Conclusions

This work provides a facile layered sorbent (PEI@Mg<sub>2</sub>SiO<sub>4</sub>) for adsorbing CO<sub>2</sub> and NACs by PEI hybridizing into Mg<sub>2</sub>SiO<sub>4</sub>. More than 11% PEI is embedded so that the sorbent contains a large numbers of reactive sites to cause an exceptional CO<sub>2</sub> capture capacity. The secondary amine group of PEI with CO<sub>2</sub> plays a key role and the experimental data fits to the DEM. The sorbent exhibits the highest adsorption capacity for CO<sub>2</sub> at 50 °C e.g. approaching 0.94 mmol/g. The sorbent regenerated by heat treatment exhibits a good stability with the adsorption-desorption cycling of CO<sub>2</sub>, e.g. decreasing by 20% for fourth cycles. In addition, the desorption rate of CO<sub>2</sub> remains more than 91% with the PEI@Mg<sub>2</sub>SiO<sub>4</sub>. Moreover, such a material appears simultaneously multifunctional, e.g. adsorption, ionic exchange and flocculation. From the adsorptions of three NACs, the PEI@Mg<sub>2</sub>SiO<sub>4</sub> exhibits a high adsorption capacity to NACs, where the electrostatic interaction plays a dominant role. The effect between the electron-donating groups and electron-withdrawing groups plays a supporting role. Then it adsorbs NP, DNP, and TNP according to the Langmuir isotherm model with a high  $q_e$  at 2.40 mmol/g, 2.66 mmol/g and 4.85 mmol/g, respectively. This work may suggest a new strategy for

development of CO<sub>2</sub> capture materials and a functionalized material for treatment of NACs wastewater.

The authors acknowledge the financial support from The Foundation of State Key Laboratory of Pollution Control and Resource Reuse (Tongji University), China (PCRRK11003).

## Acknowledgements

<sup>a</sup> State Key Laboratory of Pollution Control and Resource Reuse, College of Environmental Science and Engineering, Tongji University, Shanghai 200092, China. Tel/Fax: 86-21-65988598; E-mail: hwgao@tongji.edu.cn

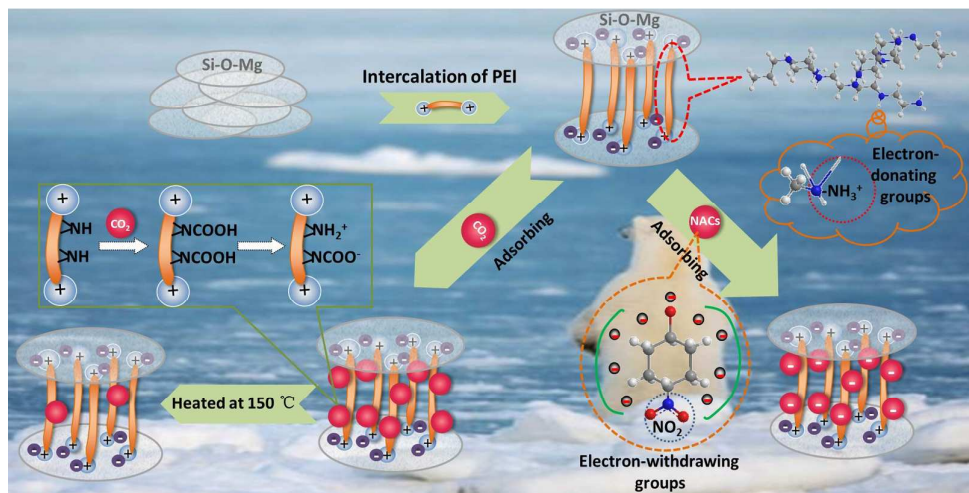
<sup>b</sup> Department of Chemistry, Key Laboratory of Functional Inorganic Materials of Anhui Province, Anhui University, Hefei 230039, P. R. China. Tel: +86-551-63861279; E-mail: jxyang@ahu.edu.cn

<sup>†</sup> Electronic Supplementary Information (ESI) available: [details of any supplementary information available should be included here]. See DOI: 10.1039/b000000x/

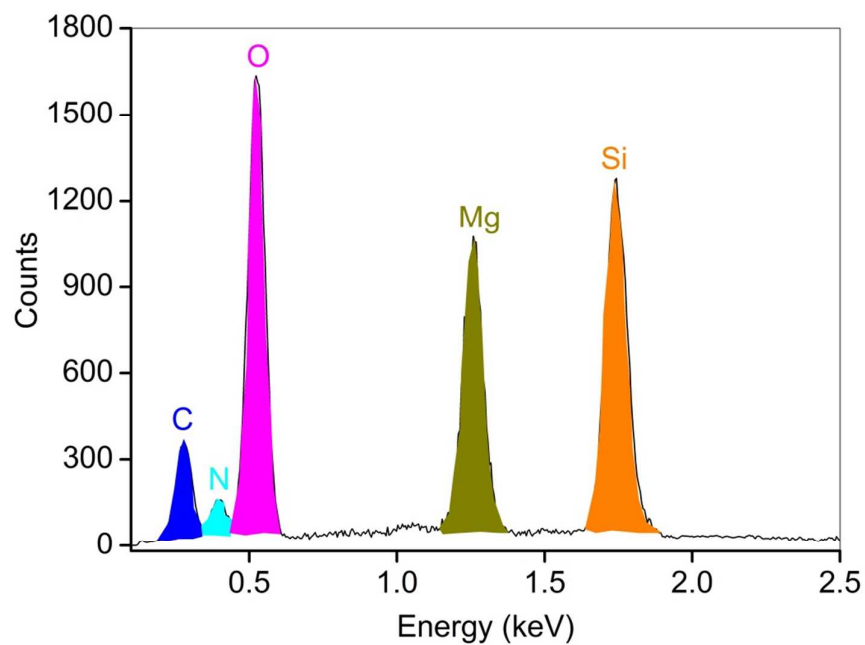
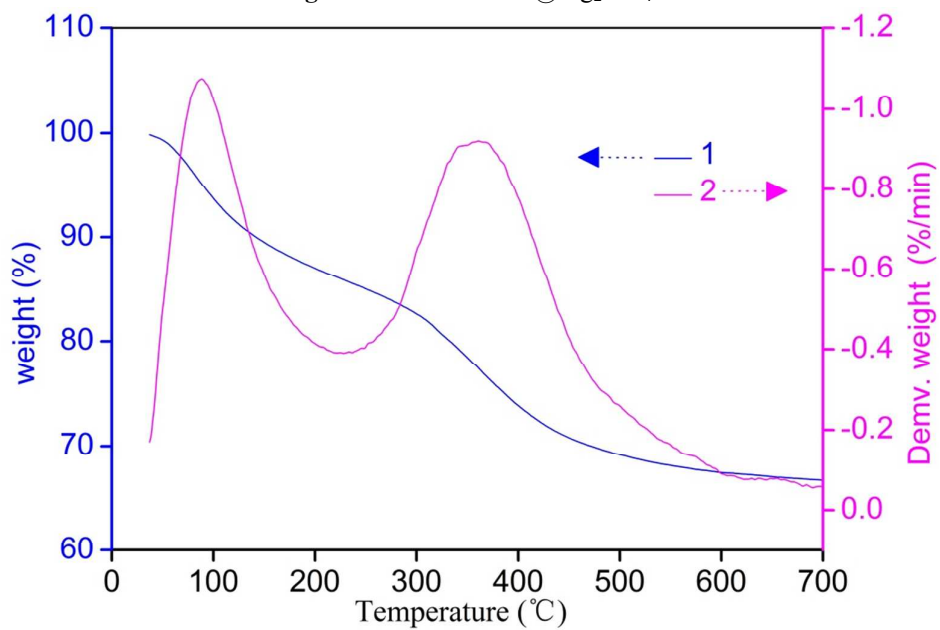
- 1 S. L. Burkett, A. Press and S. Mann, *Chem. Mater.*, 1997, **9**, 1071-1073.
- 2 Y. F. Xu, Y. C. Dai, J. Z. Zhou, Z. P. Xu, G. R. Qian and G. Q. M. Lu, *J. Mater. Chem.*, 2010, **20**, 4684-4691.
- 3 S. N. Britvin, A. Lotnyk, L. Kienle, S. V. Krivovichev and W. Depmeier, *J. Am. Chem. Soc.*, 2011, **133**, 9516-9525.
- 4 M. V. Jimenez, M. Algarra, J. J. Jimenez and M. Lamotte, *Chemosphere*, 2004, **57**, 179-186.
- 5 M. J. Manos, V. G. Petkov and M. G. Kanatzidis, *Adv. Funct. Mater.*, 2009, **19**, 1087-1092.
- 6 Y. P. Wei and H. W. Gao, *J. Mater. Chem.*, 2012, **22**, 5715-5722.
- 7 G. Decher, *Science*, 1997, **277**, 1232-1237.
- 8 M. Kimura, R. Sakai, S. Sato, T. Fukawa, T. Ikehara, R. Maeda and T. Mihara, *Adv. Funct. Mater.*, 2012, **22**, 469-476.
- 9 F. Ciesielczyk, A. Krysztalkiewicz and T. Jesionowski, *J. Mater. Sci.*, 2007, **42**, 3831-3840.
- 10 L. Estevez, R. Dua, N. Bhandari, A. Ramanujapuram, P. Wang and E. P. Giannelis, *Energy Environ. Sci.*, 2013, **6**, 1785.
- 11 X. Xue, Q. Gu, G. Pan, J. Liang, G. Huang, G. Sun, S. Ma and X. Yang, *Inorg. Chem.*, 2014, **53**, 1521-1529.
- 12 H. Cui, Y. Qian, Q. Li, Q. Zhang and J. Zhai, *Chem. Eng. J.*, 2012, **211-212**, 216-223.
- 13 G. Findenig, R. Kargl, K. Stana-Keinschek and V. Ribitsch, *Langmuir*, 2013, **29**, 8544-8553.
- 14 Y. Guo, Y. Li, T. Zhu and M. Ye, *Energ. Fuel.*, 2013, **27**, 360-366.
- 15 J. Yu, Y. Le and B. Cheng, *RSC Adv.*, 2012, **2**, 6784.



- 16 R. Wang, S. H. Guan, A. N. Sato, X. Wang, Z. Wang, R. Yang, B. S. Hsiao and B. Chu, *J. Membrane. Sci.*, 2013, **446**, 376-382.
- 17 S. B. Deng and Y. P. Ting, *Environ. Sci. Technol.*, 2005, **39**, 8490-8496.
- 18 R. Tailor, M. Abboud and A. Sayari, *Environ. Sci. Technol.*, 2014, **48**, 2025-2034.
- 19 B. J. Gao, P. F. Jiang, F. Q. An, S. Y. Zhao and Z. Ge, *Appl. Surf. Sci.*, 2005, **250**, 273-279.
- 20 N. Y. Du, H. B. Park, M. M. Dal-Cin and M. D. Guiver, *Energy Environ. Sci.*, 2012, **5**, 7306-7322.
- 21 D. W. Keith, *Science*, 2009, **325**, 1654-1655.
- 22 S. Choi, J. H. Drese and C. W. Jones, *ChemSusChem*, 2009, **2**, 796-854.
- 23 P. Ye and A. T. Lemley, *Water Res.*, 2009, **43**, 1303-1312.
- 24 N. Dey, S. K. Samanta and S. Bhattacharya, *ACS Appl. Mater. Interfaces*, 2013, **5**, 8394-8400.
- 25 A. M. Scott, L. Gorb, E. A. Mobley, F. C. Hill and J. Leszczynski, *Langmuir*, 2012, **28**, 13307-13317.
- 26 P. K. Arora, C. Sasikala and C. V. Ramana, *Appl. Microbiol. Biotechnol.*, 2012, **93**, 2265-2277.
- 27 A. J. Salter-Blanc, E. J. Bylaska, J. J. Ritchie and P. G. Tratnyek, *Environ. Sci. Technol.*, 2013, **47**, 6790-6798.
- 28 S. Shi, M. Wang, C. Chen, J. Gao, H. Ma, J. Ma and J. Xu, *Chem. Commun.*, 2013, **49**, 9591-9593.
- 29 A. Bonnefoy, S. Chiron and A. Botta, *Environ. Toxicol.*, 2012, **27**, 321-331.
- 30 Q. Wang, H. H. Tay, Z. Y. Zhong, J. Z. Luo and A. Borgna, *Energy Environ. Sci.*, 2012, **5**, 7526-7530.
- 31 G. G. Qi, Y. B. Wang, L. Estevez, X. N. Duan, N. Anako, A. H. A. Park, W. Li, C. W. Jones and E. P. Giannelis, *Energy Environ. Sci.*, 2011, **4**, 444-452.
- 32 D. H. Zhao, Y. L. Shen, Y. L. Zhang, D. Q. Wei, N. Y. Gao and H. W. Gao, *J. Mater. Chem.*, 2010, **20**, 3098-3106.
- 33 P. J. E. Harlick and A. Sayari, *Ind. Eng. Chem. Res.*, 2007, **46**, 446-458.
- 34 R. Serna-Guerrero, Y. Belmabkhout and A. Sayari, *Chem. Eng. J.*, 2010, **158**, 513-519.
- 35 G. P. Knowles, S. W. Delaney and A. L. Chaffee, *Ind. Eng. Chem. Res.*, 2006, **45**, 2626-2633.
- 36 X. L. Ma, X. X. Wang and C. S. Song, *J. Am. Chem. Soc.*, 2009, **131**, 5777-5783.
- 37 C. Chen, S. T. Yang, W. S. Ahn and R. Ryoo, *Chem. Commun.*, 2009, 3627-3629.
- 38 M. B. Yue, Y. Chun, Y. Cao, X. Dong and J. H. Zhu, *Adv. Funct. Mater.*, 2006, **16**, 1717-1722.
- 39 J. T. Wang, D. H. Long, H. H. Zhou, Q. J. Chen, X. J. Liu and L. C. Ling, *Energy Environ. Sci.*, 2012, **5**, 5742-5749.
- 40 S. M. Lee and D. Tiwari, *Appl. Clay Sci.*, 2012, **59-60**, 84-102.
- 41 S. K. Parida, S. Dash, S. Patel and B. K. Mishra, *Adv. Colloid Interface Sci.*, 2006, **121**, 77-110.
- 42 T. Kumeria, A. Santos and D. Losic, *ACS Appl. Mater. Interfaces*, 2013, **5**, 11783-11790.
- 43 C. S. Cheng, J. Deng, B. Lei, A. He, X. Zhang, L. Ma, S. Li and C. Zhao, *J. Hazard. Mater.*, 2013, **263**, 467-478.
- 44 D. Suteu, A. C. Blaga, M. Diaconu and T. Malutan, *Cent. Eur. J. Chem.*, 2013, **11**, 2048-2057.
- 45 F. Rezaei, R. P. Lively, Y. Labreche, G. Chen, Y. Fan, W. J. Koros and C. W. Jones, *ACS Appl. Mater. Interfaces*, 2013, **5**, 3921-3931.
- 46 J. Y. Kim, J. Kim, S. T. Yang and W. S. Ahn, *Fuel*, 2013, **108**, 515-520.
- 47 S. L. Burkett, A. Press and S. Mann, *Chem. Mater.*, 1997, **9**, 1071-1073.
- 48 A. Zukal, I. Dominguez, J. Mayerova and J. Cejka, *Langmuir*, 2009, **25**, 10314-10321.
- 49 S. T. Yang, J. Y. Kim, J. Kim and W. S. Ahn, *Fuel*, 2012, **97**, 435-442.
- 50 J. Yu, S. Liu and H. Yu, *J. Catal.*, 2007, **249**, 59-66.
- 51 N. P. Wickramaratne and M. Jaroniec, *J. Mater. Chem. A*, 2013, **1**, 112.
- 52 M. M. Gui, Y. X. Yap, S.-P. Chai and A. R. Mohamed, *Int. J. Greenh. Gas Control*, 2013, **14**, 65-73.
- 53 S. B. Yang, L. Zhan, X. Y. Xu, Y. L. Wang, L. C. Ling and X. L. Feng, *Adv. Mater.*, 2013, **25**, 2130-2134.
- 54 Q. Wang, Y. S. Gao, J. Z. Luo, Z. Y. Zhong, A. Borgna, Z. H. Guo and D. O'Hare, *RSC Adv.*, 2013, **3**, 3414-3420.
- 55 A. Chakradhar and U. Burghaus, *Surf. Sci.*, 2013, **616**, 171-177.
- 56 Z. Chen, S. Deng, H. Wei, B. Wang, J. Huang and G. Yu, *ACS Appl. Mater. Interfaces*, 2013, **5**, 6937-6945.
- 57 P. Bollini, N. A. Brunelli, S. A. Didas and C. W. Jones, *Ind. Eng. Chem. Res.*, 2012, **51**, 15153-15162.
- 58 N. Chiron, R. Guilet and E. Deydier, *Water Res.*, 2003, **37**, 3079-3086.
- 59 Z.-h. Tang, Z. Han, G.-z. Yang, B. Zhao, S.-l. Shen and J.-h. Yang, *New Carbon Mater.*, 2013, **28**, 55-60.
- 60 F. Durán-Muñoz, I. C. Romero-Ibarra and H. Pfeiffer, *J. Mater. Chem. A*, 2013, **1**, 3919.
- 61 A. Garcia-Gallastegui, D. Iruetagoiena, M. Mokhtar, A. M. Asiri, S. N. Basahel, S. A. Al-Thabaiti, A. O. Alyoubi, D. Chadwick and M. S. P. Shaffer, *J. Mater. Chem.*, 2012, **22**, 13932-13940.
- 62 A. Garcia-Gallastegui, D. Iruetagoiena, V. Gouvea, M. Mokhtar, A. M. Asiri, S. N. Basahel, S. A. Al-Thabaiti, A. O. Alyoubi, D. Chadwick and M. S. P. Shaffer, *Chem. Mater.*, 2012, **24**, 4531-4539.
- 63 M. C. Hermosin, I. Pavlovic, M. A. Ulibarri and J. Cornejo, *Water Res.*, 1996, **30**, 171-177.
- 64 Q. S. Liu, T. Zheng, P. Wang, J. P. Jiang and N. Li, *Chem. Eng. J.*, 2010, **157**, 348-356.
- 65 A. Kumar, S. Kumar and D. Gupta, *J. Hazard. Mater.*, 2007, **147**, 155-166.
- 66 M. G. Roberts, C. L. Rugh, H. Li, B. J. Teppen and S. A. Boyd, *Environ. Sci. Technol.*, 2007, **41**, 1641-1645.
- 67 T. B. Hofstetter, R. P. Schwarzenbach and S. B. Haderlein, *Environ. Sci. Technol.*, 2003, **37**, 519-528.
- 68 A. Reynal, A. Forneli, E. Martinez-Ferrero, A. Sanchez-Diaz, A. Vidal-Ferran, B. C. O'Regan and E. Palomares, *J. Am. Chem. Soc.*, 2008, **130**, 13558-13567.
- 69 M. Amara and H. Kerdjoudj, *Desalination*, 2003, **155**, 79-87.
- 70 F. An, B. Gao and X. Feng, *J. Hazard. Mater.*, 2008, **157**, 286-292.
- 71 A. A. M. Daifullah and B. S. Girgis, *Water Res.*, 1998, **32**, 1169-1177.

Electronic Supplementary Information (ESI)**PEI@Mg<sub>2</sub>SiO<sub>4</sub>: an efficient carbon dioxide and nitrophenol compounds adsorbing material****A table of contents entry****PEI@Mg<sub>2</sub>SiO<sub>4</sub>: an efficient carbon dioxide and nitrophenol compounds adsorbing material**

Figures S1 – S3 and Table S1

Fig. S1 EDX of the PEI@Mg<sub>2</sub>SiO<sub>4</sub>.Fig. S2 TGA (1) and DTA (2) of the PEI@Mg<sub>2</sub>SiO<sub>4</sub>.

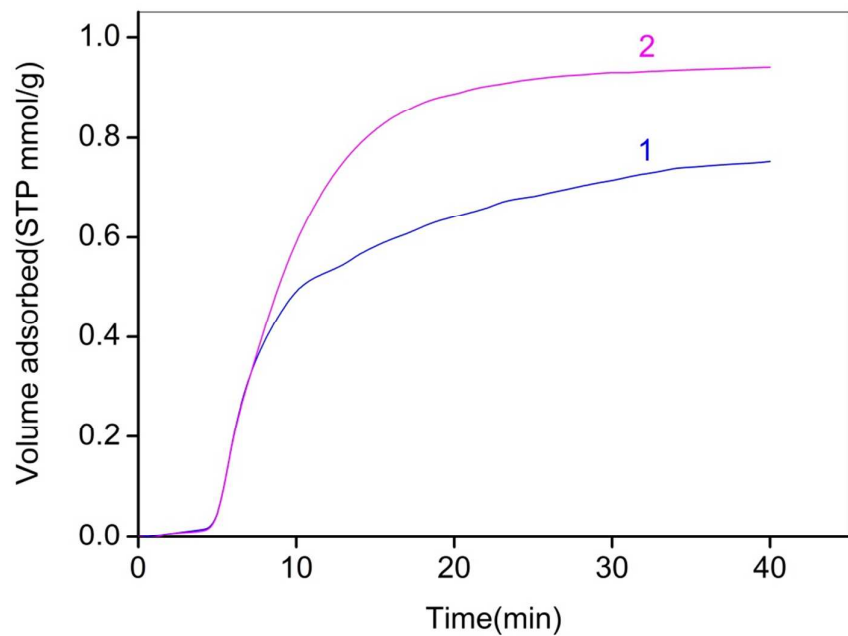


**Fig. S3** Effect of time on the adsorption of  $CO_2$  absorption for  $Mg_2SiO_4$  (1) and the  $PEI@Mg_2SiO_4$  (2) at  $50\text{ }^\circ\text{C}$ .

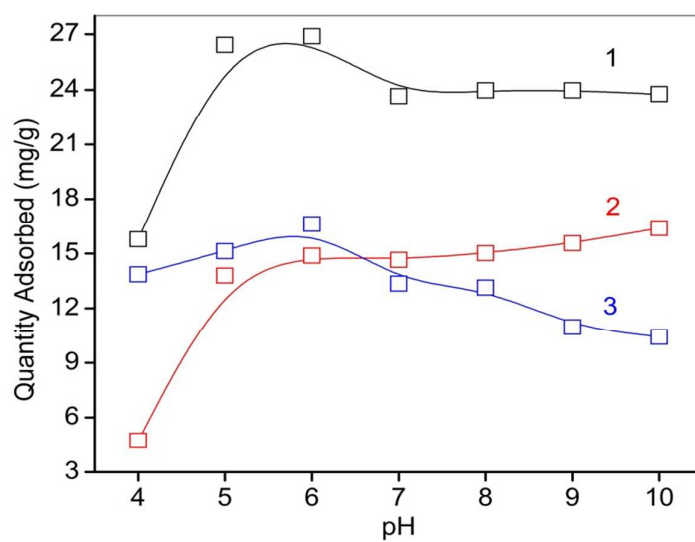


**Fig. S4** The sorption curve of NACs (1-NP, 2-DNP and 3-TNP) to the  $PEI@Mg_2SiO_4$  material at different pH.

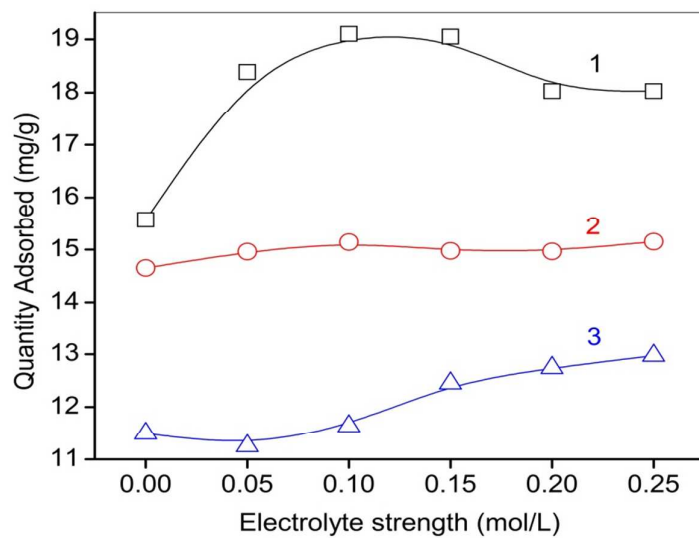


**Fig. S5** Effect of ionic strength on the adsorption of NACs (1-NP, 2-DNP and 3-TNP) to the PEI@Mg<sub>2</sub>SiO<sub>4</sub> material

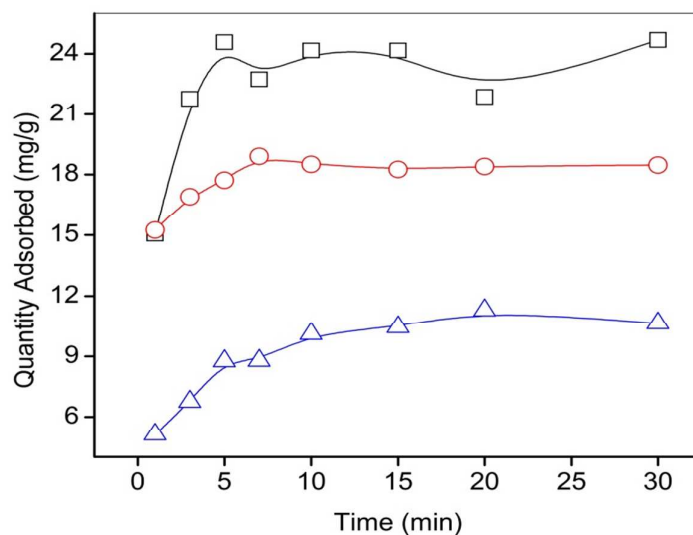


**Fig. S6** The sorption curve of NACs (1-NP, 2-DNP and 3-TNP) to the PEI@Mg<sub>2</sub>SiO<sub>4</sub> material at different times

**Table. S1** Change of C and N contents in the PEI@Mg<sub>2</sub>SiO<sub>4</sub>

	C %	N %	H %
PEI@Mg <sub>2</sub> SiO <sub>4</sub>	7.078	3.811	4.200

**Table. S2** Parameters of the DEM Kinetic Model obtained for CO<sub>2</sub> adsorption on the PEI@Mg<sub>2</sub>SiO<sub>4</sub>

Temperature (°C)	$q_e$ (mg/g)	Fast adsorption		Slow adsorption		$R^2$
		$D_1$ (mg/g)	$K_1$ (min <sup>-1</sup> )	$D_2$ (mg/g)	$K_2$ (min <sup>-1</sup> )	
25	35.6	18.4	0.32	17.5	0.06	0.99
50	42.3	24.1	0.15	24.1	0.15	0.98
75	29.3	15.5	0.89	12.5	1.71	0.97
100	15.2	0.58	0.57	7.2	1.72	0.95